ACS APPLIED MATERIALS & INTERFACES

Research Article

www.acsami.org

Efficient Photoinduced Charge Accumulation in Reduced Graphene Oxide Coupled with Titania Nanosheets To Show Highly Enhanced and Persistent Conductance

Xingke Cai,[†,‡] Nobuyuki Sakai,[†] Tadashi C. Ozawa,[†] Asami Funatsu,[†] Renzhi Ma,[†] Yasuo Ebina,[†] and Takayoshi Sasaki*[,†,‡]

[†]International Center for Materials Nanoarchitectonics, National Institute for Materials Science, 1-1 Namiki, Tsukuba, Ibaraki 305-0044, Japan

[‡]Graduate School of Pure and Applied Sciences, University of Tsukuba, 1-1-1 Tennodai, Tsukuba, Ibaraki 305-8571, Japan

Supporting Information

ABSTRACT: Tuning of the electrical properties of graphene via photoexcitation of a heteroassembled material has started to attract attention for electronic and optoelectronic applications. Actually photoinduced carrier doping from the hexagonal boron nitride (h-BN) substrate greatly modulated the transport property of the top layer graphene, showing promising potential for this approach. However, for practical applications, the large scale production of this two-dimensional heterostructure is needed. Here, a superlattice film constructed from reduced graphene oxide (rGO) and photoactive titania nanosheets ($Ti_{0.87}O_2^{0.52-}$) was employed as a channel to construct a field effect transistor (FET) device, and its UV light response on the electrical transport property was examined. The UV light illumination induced significant improvement of the electrical conductance by ~7 times on the basis of simultaneous enhancements of the electron carrier concentration and its mobility in rGO. Furthermore, the polarity of the FET response changed from ambipolar to n-type unipolar. Such modulated properties persisted in vacuum even after the UV light was turned off. These interesting behaviors may be explained in terms of photomodulation effects from $Ti_{0.87}O_2^{0.52-}$ nanosheets. The photoexcited electrons in $Ti_{0.87}O_2^{0.52-}$ are injected into rGO to increase the electron carrier concentration as high as 7.6×10^{13} cm^{-2}. On the other hand, the holes are likely trapped in the $Ti_{0.87}O_2^{0.52-}$ nanosheets. These photocarriers undergo reduction and oxidation of oxygen and water molecules adsorbed in the film, respectively, which act as carrier scattering centers, contributing to the enhancement of the carrier mobility. Since the film likely contains more water molecules than oxygen, upon extinction of UV light, a major portion of electrons (~80% of the concentration at the UV off) survives in rGO, showing the highly enhanced conductance for days. This surpassing photomodulated FET response and its persistency observed in the present superlattice system of rGO/$Ti_{0.87}O_2^{0.52-}$ are noteworthy compared with previous studies such as the device with a heteroassembly of graphene/h-BN.

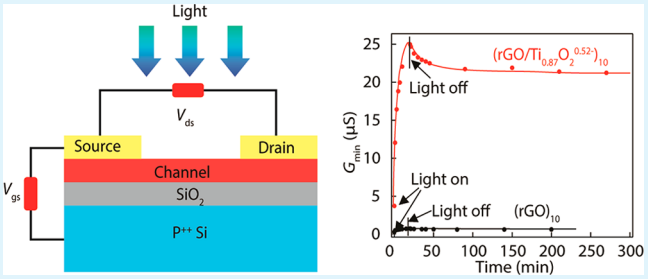

KEYWORDS: *reduced graphene oxide, titania nanosheet, superlattice, charge accumulation, photomodulation*

INTRODUCTION

The discovery of graphene[1] and its novel properties[1−6] have sparked an enormous research boom, which has further extended over a range of two-dimensional (2D) materials based on metal oxides,[7−9] hydroxides,[7] and nitrides,[10,11] as well as chalcogenides.[12−14] The unilamellar 2D sheets or stacks of a few layers frequently exhibit intriguing properties, arising from their nanoscale thickness and an ultimately large surface area. Thus, many new applications are being developed on the basis of the distinctive functionalities, which are difficult to realize in bulk materials.[2,5,7,8,13,14]

Among a wide range of research directions relating to graphene and its analogues, the organization of heterostructures with multiple 2D materials has emerged as a promising research front. Synergetic electronic, magnetic, or chemical interactions between different 2D materials are expected to develop new or greatly enhanced functionalities. Several reports have demonstrated the effectiveness of this strategy.[8,11,15−18] Among nearly limitless combinations, one of the promising targets is the modulation or tuning of the superior electrical properties of graphene by combining it with other types of 2D materials. For example, a vertically aligned n-channel field effect transistor (FET) was fabricated by sandwiching a few layers of MoS_2 as the semiconducting channel between a graphene sheet and a metal thin film, achieving a high device performance, an on−off ratio of $>10^3$, and a high current density of up to 5000 A cm^{-2} at room temperature.[18] A hexagonal boron nitride (h-BN)/graphene/h-BN structure with a unique edge contact geometry

Received: March 10, 2015
Accepted: May 6, 2015
Published: May 6, 2015

DOI: 10.1021/acsami.5b02107
ACS Appl. Mater. Interfaces 2015, 7, 11436−11443

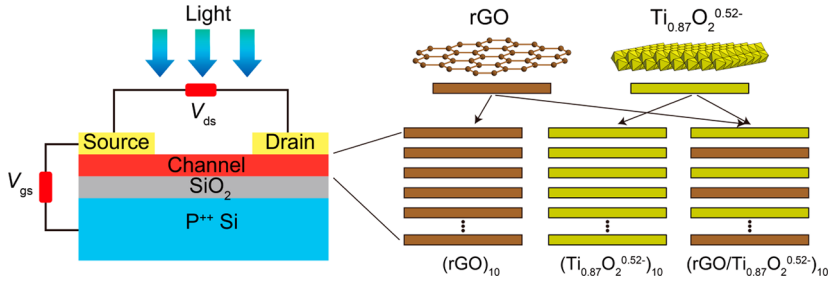

Figure 1. Schematic diagram of a FET device based on $(rGO)_{10}$, $(Ti_{0.87}O_2^{0.52-})_{10}$, and $(rGO/Ti_{0.87}O_2^{0.52-})_{10}$ films under UV illumination. The various multilayer and superlattice films composed of rGO and $Ti_{0.87}O_2^{0.52-}$ nanosheets were fabricated on a Si substrate with 300-nm-thick SiO_2. The metallic terminals (5 nm Ti/50 nm Au) were deposited on top of the films by electron beam deposition, acting as source and drain electrodes, whereas the heavily doped Si was used as the back gate electrode.

was found to achieve low-temperature ballistic transport over a distance longer than 15 μm, and its room temperature mobility is comparable to the theoretical phonon-scattering limit due to the reduced impurity scattering and contact resistance.[16] Recent work based on graphene/h-BN heterostructures demonstrated that photoinduced carrier doping from the defects of h-BN into graphene could modify the electrical properties of graphene, which indicates the potential for new scientific studies and applications.[19] However, h-BN is an insulator with a large bandgap of 5.2 eV, which can absorb only ultraviolet (UV) light at high energy (λ < 240 nm). The observed modulation is associated with electrons transferred from h-BN trapped at impurity levels. This photoinduced doping effect resulting from an impurity is typically rather modest.

One important class of 2D materials is oxide nanosheets. A wide variety of layered metal oxides have been delaminated into colloidal elementary layers through a soft-chemical route via intercalation/swelling.[7,20,21] The obtained unilamellar 2D layers are monodispersed polyanionic sheets, and they can be assembled layer-by-layer into well-organized nanostructured films by solution-based processes, such as electrostatic sequential adsorption[22] and the Langmuir–Blodgett method.[23] Of particular interest is the titania nanosheet, which acts as a wide-gap semiconductor, exhibiting useful physical and chemical properties. The titania nanosheet efficiently absorbs UV light and exhibits high photocatalytic and dielectric properties.[9]

We recently fabricated a superlattice film of alternately stacked graphene oxide (GO) and titania nanosheets of $Ti_{0.87}O_2^{0.52-}$ and demonstrated that GO could be effectively converted into a reduced form (rGO) upon exposure to UV light due to the photocatalytic activity of $Ti_{0.87}O_2^{0.52-}$.[24] Therefore, it is important and meaningful to explore the modulation of the electrical behavior of such a FET device based on the film of $rGO/Ti_{0.87}O_2^{0.52-}$ upon light illumination. The strong absorption of UV light by $Ti_{0.87}O_2^{0.52-}$ nanosheets and the intimate stacking with rGO at a molecular scale is expected to facilitate the injection of photogenerated carriers. Efficient and controllable photoinduced modulation of the transport properties is expected because of the alternate assembly of molecularly thin 2D materials.

EXPERIMENTAL SECTION

Preparation and Characterization of Films. GO was prepared by a modified Hummers method,[25] whereas titania nanosheets, $Ti_{0.87}O_2^{0.52-}$, were derived from $K_{0.8}Ti_{1.73}Li_{0.27}O_4$ through a soft-chemical exfoliation process.[26] AFM observations revealed that these nanosheets have a typical thickness of 0.8 and 1.1 nm, with an average lateral size of 1 μm and 300 nm, respectively (Supporting Information Figure S1). The multilayer and superlattice films, such as $(PDDA/GO)_{10}$, where PDDA denotes poly(diallyldimethylammonium chloride), $(PDDA/Ti_{0.87}O_2^{0.52-})_{10}$, and $(PDDA/GO/PDDA/Ti_{0.87}O_2^{0.52-})_{10}$, were assembled in a layer-by-layer manner on a heavily doped Si substrate, with a 300-nm-thick SiO_2 layer, through sequential adsorption using PDDA as the cationic linker. The successful fabrication of the multilayers was indicated by the progressive enhancement of UV–vis absorbance during the fabrication process on the quartz substrates (Supporting Information Figure S2). The $(PDDA/Ti_{0.87}O_2^{0.52-})_{10}$ and $(PDDA/GO/PDDA/Ti_{0.87}O_2^{0.52-})_{10}$ films were exposed to UV light for 48 h to promote photocatalytic reduction of GO to rGO and decomposition of the PDDA. The UV treatment was the same as that employed in our previous study for the film of $(PDDA/Ti_{0.87}O_2^{0.52-})_{10}$, where the total removal of PDDA was confirmed.[27] To achieve a similar reduction extent with the photoreduced $(rGO/Ti_{0.87}O_2^{0.52-})_{10}$ film, the $(PDDA/GO)_{10}$ film was heated at 400 °C for 1 h under vacuum to obtain the $(rGO)_{10}$ film. The prepared samples were kept in ambient air prior to electrical measurements.

Electrical Transport Property Measurements. The transistor action and its photoelectrical performance were examined on FET devices fabricated with the films as the channel using the heavily doped Si substrate as the gate electrodes, as is commonly employed. Ti/Au (5 nm/50 nm) electrodes were deposited on the films via electron beam deposition with a channel length (L) and width (W) of 40 and 400 μm, respectively. The measurements were carried out under vacuum (<10^{-3} Pa), using a semiconductor parameter analyzer (Keithley 4200-SCS, Keithley Instruments Inc.) with a low-temperature probe system from Nagase Electronic Equipment Service. The voltage difference between the source and drain (V_{ds}) was set at 1 V. A xenon lamp (XEF-501S, San-ei Electric) with an optical fiber was used as the light source. The light was guided through the optical filter and irradiated the device vertically when the photomodulation was monitored. The light intensity was calibrated by a spectroradiometer (USR-45, Ushio). To examine the photomodulation of the transistor action, we recorded various data, such as I_{ds}–V_{ds} and G–V_{gs} relationships, (I_{ds}: current between the source and drain electrodes, V_{gs}: voltage between the source and gate electrodes) in the dark immediately after turning off the light.

RESULTS AND DISCUSSION

The multilayer films $(rGO/Ti_{0.87}O_2^{0.52-})_{10}$, $(rGO)_{10}$, and $(Ti_{0.87}O_2^{0.52-})_{10}$ were obtained by a layer-by-layer method followed by the reduction processes. Compositional and structural aspects of the films were reported in our previous work.[24] The thickness of the films estimated from XRD data was 18.4, 11.4, and 9.8 nm, respectively. In this paper, we focus on the photomodulation effects on the electrical transport properties of the films.

DOI: 10.1021/acsami.5b02107
ACS Appl. Mater. Interfaces 2015, 7, 11436–11443

The FET devices were fabricated employing the resulting films as channel materials, as illustrated in Figure 1. The Si substrate works as the gate electrode, whereas metallic terminals (Ti/Au, thickness: 5/50 nm) deposited on top of the films act as source and drain electrodes. An ohmic response, or a linear current (I_{ds})−voltage (V_{ds}) relationship, was observed for the films of $(rGO/Ti_{0.87}O_2^{0.52-})_{10}$ and $(rGO)_{10}$, suggesting that the energy barriers at the contacts are negligible (Figure 2). In contrast, the $I_{ds}-V_{ds}$ curve for the $(Ti_{0.87}O_2^{0.52-})_{10}$

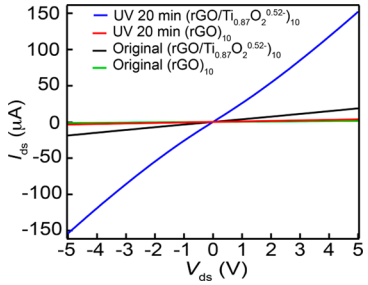

Figure 2. $I_{ds}-V_{ds}$ curves for $(rGO)_{10}$ and $(rGO/Ti_{0.87}O_2^{0.52-})_{10}$ films before and after the UV illumination. The measurement was performed at V_{gs} = 0 V for both films. The UV light used here ranged from 270 to 400 nm, with an intensity of 14 mW cm^{-2}, and the illumination time was 20 min. The data for the $(rGO)_{10}$ film are nearly superimposable with each other because of a negligible change before and after the UV treatment. In contrast, the resistance for $(rGO/Ti_{0.87}O_2^{0.52-})_{10}$ was significantly reduced after the UV treatment.

film could not be obtained with our instrument because of the highly insulating character of this nanosheet.[28] The resistances for the as-fabricated films of $(rGO)_{10}$ and $(rGO/Ti_{0.87}O_2^{0.52-})_{10}$ were 3.3×10^7 and 2.8×10^6 Ω sq^{-1}, respectively. Considering the highly insulating nature of the $Ti_{0.87}O_2^{0.52-}$ nanosheet, it is reasonable to assume that the rGO layer in the $(rGO/Ti_{0.87}O_2^{0.52-})_{10}$ film primarily contributes to the conductive properties.

Then, the devices were illuminated with UV light (270−400 nm, 14 mW cm^{-2}) for ∼20 min under vacuum (<10^{-3} Pa). After this treatment, the resistance for the $(rGO/Ti_{0.87}O_2^{0.52-})_{10}$ film significantly decreased to ∼$^1/_7$ to 3.9×10^5 Ω sq^{-1}, whereas that of the $(rGO)_{10}$ film changed negligibly. These films have been fully reduced through the aforementioned treatments involving photocatalytic or thermal reduction, excluding a possibility for further reduction under the UV illumination during the electrical measurements.[24] We also carried out the measurements under different illumination conditions (Supporting Information Figure S3). The device with the $(rGO/Ti_{0.87}O_2^{0.52-})_{10}$ film exhibited only a slight change in conductance under visible light, whereas a noticeable enhancement was observed under UV light. The conductance enhancement was accelerated at a higher intensity. These data indicate that the photoinduced modulation effects observed for $(rGO/Ti_{0.87}O_2^{0.52-})_{10}$ film should be associated with carriers generated in the $Ti_{0.87}O_2^{0.52-}$ nanosheet via bandgap excitation.

Typical conductance−gate voltage ($G-V_{gs}$) curves for the $(rGO/Ti_{0.87}O_2^{0.52-})_{10}$ and $(rGO)_{10}$ films before and after the UV light treatment are compared in Figure 3. The conductive nature of the $(rGO/Ti_{0.87}O_2^{0.52-})_{10}$ film changed from ambipolarity to n-type unipolarity upon UV light treatment (Figure 3a), while the ambipolarity of the $(rGO)_{10}$ film remained largely unchanged (Figure 3b). This result for the $(rGO)_{10}$ film is compatible with previous reports on FETs based on graphene as well as rGO prepared by various processes, where the ambipolarity remained unchanged after light illumination.[19,29] Thus, the photoresponse of the conductive behavior to the n-type unipolarity observed in $(rGO/Ti_{0.87}O_2^{0.52-})_{10}$ may be unique in a number of the graphene-based devices.

The exposure to UV light generates excited electrons and holes in the $Ti_{0.87}O_2^{0.52-}$ nanosheets of the superlattice film via bandgap excitation. Because the conduction band edge of the $Ti_{0.87}O_2^{0.52-}$ nanosheet is more negative than that of rGO,[30,31] the electrons are transferred to rGO. Similar electron transfer was reported in heterosystems of TiO_2 nanoparticles and graphene.[32−35] Furthermore, under the UV illumination, the $Ti_{0.87}O_2^{0.52-}$ nanosheet shows a strong photocatalytic ability to remove species such as water and oxygen molecules, which have a p-type doping effect.[1,36,37] These species are easily adsorbed on the film surface and are difficult to remove by normal evacuation. Furthermore, the film contains water molecules or oxonium ions in the interlayer gallery because of the solution-based fabrication process. Under UV illumination, excited electrons can reduce molecular oxygen to be desorbed, and holes may decompose water molecules in the film. The n-type conductive polarity observed for the $(rGO/Ti_{0.87}O_2^{0.52-})_{10}$ film upon UV irradiation may be understood in terms of these two effects.

To gain further insights into these aspects, the $G-V_{gs}$ curves of the $(rGO)_{10}$ and $(rGO/Ti_{0.87}O_2^{0.52-})_{10}$ films were recorded by sweeping the gate voltage in the forward (from −100 to 100 V) and reverse (from 100 to −100 V) directions in the dark before and after the UV light treatment. The gate voltage values at the charge neutrality point (CNP), $V_{g,min}$, for the $(rGO)_{10}$ film before the UV light treatment were different between the

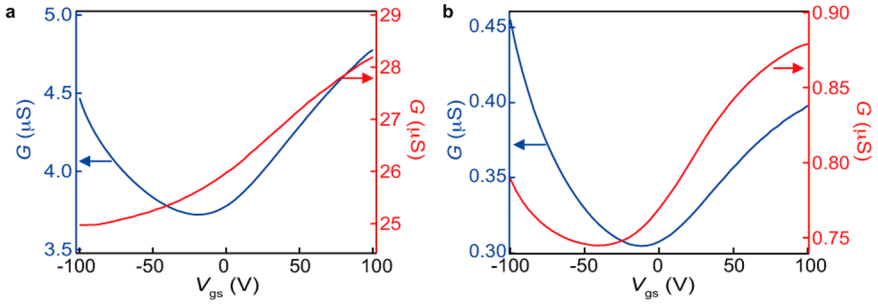

Figure 3. $G-V_{gs}$ curves before and after UV illumination process: (a) $(rGO/Ti_{0.87}O_2^{0.52-})_{10}$ and (b) $(rGO)_{10}$. The blue traces denote the curves recorded before light illumination, whereas the red traces denote the curves recorded after UV (14 mW cm^{-2}) illumination for 20 min. The measurements were performed at V_{ds} = 1 V for both films.

DOI: 10.1021/acsami.5b02107
ACS Appl. Mater. Interfaces 2015, 7, 11436−11443

forward and reverse sweeping (−12 and 14 V, respectively; Figure 4a). The $G-V_{gs}$ curves did not change significantly after

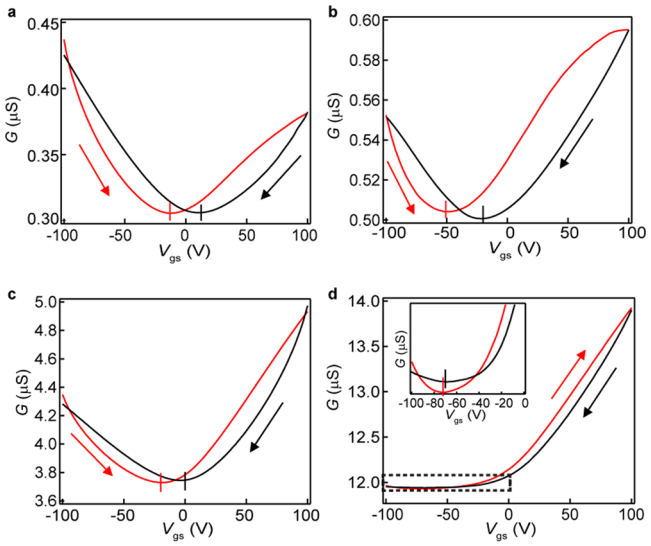

Figure 4. $G-V_{gs}$ curves for (a, b) $(rGO)_{10}$ and (c, d) $(rGO/Ti_{0.87}O_2^{0.52-})_{10}$ films before and after UV illumination (14 mW cm^{-2}) for 1 min. The data were obtained during the forward sweeping (red traces, from −100 to 100 V) and the reverse sweeping (black traces, from 100 to −100 V). Inset in part d shows a magnified drawing of the curves in the area designated by the rectangular dotted frame.

the UV exposure for 1 min, although the $V_{g,min}$ values shifted to be negative, indicating n-type doping (Figure 4b). The hysteresis was still observed after 20 min of UV light treatment (Supporting Information Figure S4). The hysteresis observed in FET devices using a channel based on nanomaterials is typically caused by the adsorption of water or molecular oxygen onto the channel surface,[38−40] which might be polarized under an applied electric field. The hysteresis observed should be attributable to these effects. In contrast, the hysteresis of the $(rGO/Ti_{0.87}O_2^{0.52-})_{10}$ film was smaller than that of $(rGO)_{10}$, and the $V_{g,min}$ values (−20 and 0 V for the forward and reverse sweeping, respectively) were more negative than the corresponding values for $(rGO)_{10}$ (Figure 4c). One minute of UV light treatment suppressed the hysteresis of the $(rGO/Ti_{0.87}O_2^{0.52-})_{10}$ film to 2 V and increased the conductance (Figure 4d). The suppressed hysteresis observed for the $(rGO/Ti_{0.87}O_2^{0.52-})_{10}$ film supports the notion mentioned above that removing adsorbed species such as oxygen and water molecules takes place due to the strong photocatalytic activity of $Ti_{0.87}O_2^{0.52-}$ nanosheets. As will be shown below, the carrier mobility enhancement was confirmed in this system.

Graphene and its derivatives have great potential as electronic and optoelectronic materials. However, their electrical properties are considerably influenced by the atmosphere; water and oxygen molecules easily adsorb on the device. Many methods have been proposed to recover their intrinsic properties, such as annealing in reducing atmosphere[11] and shielding them with h-BN nanosheets.[16] The present system, rGO coupled with photoresponsive $Ti_{0.87}O_2^{0.52-}$ nanosheets, provides another facile and effective way to exclude the influence of the atmosphere.

Series of $G-V_{gs}$ curves in the forward sweep process for the films of $(rGO/Ti_{0.87}O_2^{0.52-})_{10}$ and $(rGO)_{10}$ were collected in the dark immediately after UV illumination (14 mW cm^{-2}) for a certain period (Supporting Information Figure S5). From the obtained $G-V_{gs}$ curves, the conductance at CNP (G_{min}), gate voltage at CNP ($V_{g,min}$), carrier mobility (μ), and carrier concentration at CNP (n_i) upon illumination, as well as the

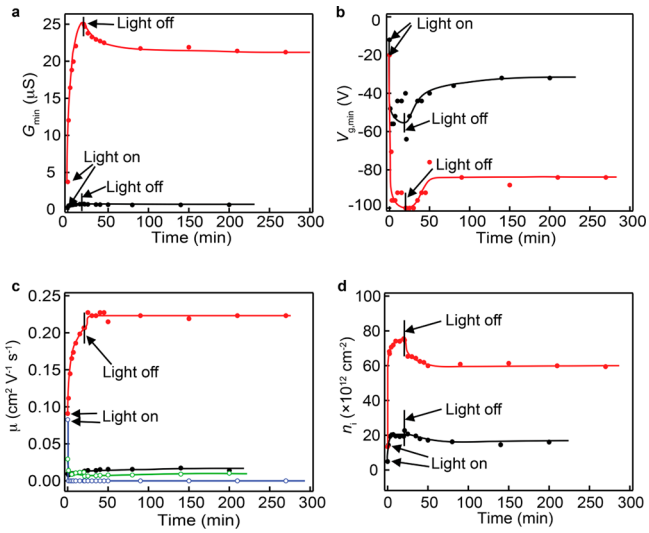

Figure 5. Changes of (a) conductance at CNP (G_{min}), (b) gate voltage at CNP ($V_{g,min}$), (c) carrier mobility (μ) for electrons (●) and holes (○), and (d) carrier concentration at CNP (n_i) for $(rGO/Ti_{0.87}O_2^{0.52-})_{10}$ (red) and $(rGO)_{10}$ (black) upon UV illumination and the subsequent dark process. The blue and green trace in (c) stand for the change of the hole carrier mobility for $(rGO)_{10}$ and $(rGO/Ti_{0.87}O_2^{0.52-})_{10}$.

subsequent dark process, were deduced (Figure 5). G_{min} is related to the carrier concentrations and mobility as follows:

$$G_{min} = (I_{ds})_{min}/V_{ds} = [n_i e(\mu_e + \mu_h)W]/(V_{ds}/E) = n_i e(\mu_e + \mu_h)(W/L) \quad (1)$$

where E is the electric field, n_i is the surface charge density, μ_e and μ_h are the related electron and hole carrier mobilities, respectively, and W and L are the channel width and length, respectively. The carrier mobility (μ) was obtained using the derivative of the Drude equation,[11,39] and the charge density (n_i) was estimated according to eq 1. G_{min} of the $(rGO/Ti_{0.87}O_2^{0.52-})_{10}$ film was noticeably enhanced as the UV illumination time increased (Figure 5a). In contrast, such an enhancement of G_{min} was observed only to a limited extent for the $(rGO)_{10}$ film. After illumination for 20 min, G_{min} of the $(rGO/Ti_{0.87}O_2^{0.52-})_{10}$ film increased from 3.8 to 25 μS, an increase of 7-fold.[41] This change is ∼50 times higher than that reported previously for graphene-based FETs,[19,29] which exhibited only modest enhancements upon exposure to visible light.

First, let's discuss the differences between the films of $(rGO/Ti_{0.87}O_2^{0.52-})_{10}$ and $(rGO)_{10}$. It is clear that the superior conductance for $(rGO/Ti_{0.87}O_2^{0.52-})_{10}$ is attributable to the higher carrier mobility and concentration. The largely enhanced carrier mobility, or reduced energy barriers for carriers transferring between the rGO sheets, may be attributed to effective dielectric shielding from the high-κ $Ti_{0.87}O_2^{0.52-}$ nanosheets, which intimately sandwich rGOs at a molecular level, and the above-mentioned removal of oxygen and water molecules in the film, which are known to act as carrier

DOI: 10.1021/acsami.5b02107
ACS Appl. Mater. Interfaces 2015, 7, 11436−11443

scattering impurities. The noticeable increase in carrier concentration for the $(rGO/Ti_{0.87}O_2^{0.52-})_{10}$ film can be ascribed to the efficient transfer of electrons generated in the $Ti_{0.87}O_2^{0.52-}$ nanosheet to rGO. $V_{g,min}$ of the $(rGO/Ti_{0.87}O_2^{0.52-})_{10}$ film gradually shifted negative upon UV illumination (Figure 5b), which is a typical phenomenon related to electron doping. The value changed by 80 V from −20 to −100 V after 20 min of UV illumination, leading to the unipolar response. This n-doping effect is considerably smaller for $(rGO)_{10}$ without a coupled photoresponsive material.

As the UV illumination time increased, both μ_e and n_i for $(rGO/Ti_{0.87}O_2^{0.52-})_{10}$ increased, whereas μ_h decreased to nearly zero (Figure 5c,d). Hence, the increase in the carrier concentration (n_i) mainly contributes to the improved conductance G_{min} during the UV illumination process. A significant increase in electron carrier mobility (μ_e) (Figure 5c) was observed, which should be accounted for by the effects above, removal of the adsorbed water and oxygen.

Among these photoinduced modulation effects, one of the most marked features is the extremely high electron carrier concentration, reaching 7.6×10^{13} cm^{-2}. To the best of our knowledge, this concentration is the highest value among reported data for graphene- or rGO-based FETs, many of which exhibited an electron concentration that was 1 order of magnitude lower.[1,4,29,36,42−45] This remarkably high accumulation of electrons in rGO in the present system is due to the efficient transfer of excited electrons generated in $Ti_{0.87}O_2^{0.52-}$ nanosheets to rGO. The charge induced by the gate potential is considerably smaller than the electron carrier concentration of 7.6×10^{13} cm^{-2} observed. A value of $\sim 1 \times 10^{13}$ cm^{-2} at a gate voltage of 100 V is expected on the basis of the standard estimation for the present system with 300-nm-thick SiO_2 as a gate insulator.[1] This large difference may account for the rather broad and n-unipolar response observed for the $G-V_{gs}$ curves observed (Supporting Information Figure S5). The apparent unipolarity may be understood, considering the fact that the number of holes induced by the gate potential is also significantly smaller than that of the photoinduced accumulated electrons.

Interestingly, the photoinduced, highly enhanced transport properties of rGO coupled with the $Ti_{0.87}O_2^{0.52-}$ nanosheets were nearly unchanged after turning off the UV light. Although the conductance exhibited a modest ∼10% decay upon UV extinction, the residual high value remained constant for at least 4 days (Figure 6).[46] Although we could not record data for a longer duration due to the limitation of the instrument, we expect that the conductance will not exhibit a noticeable decay for a prolonged duration as long as it is kept in vacuum. The carrier concentration exhibited a similar trend; namely, it decreased to ∼80% at the termination of UV illumination but remained nearly constant after that. The decrease can be understood by recombination with the remaining holes trapped in $Ti_{0.87}O_2^{0.52-}$ nanosheets, or those not consumed in the photocatalytic decomposition of water. The electron carrier mobility increased from 0.21 to 0.22 cm^2 V^{-1} s^{-1} when turning off the UV lamp (Figure 5c), which may be ascribed to the decreased carrier−carrier scattering.[47]

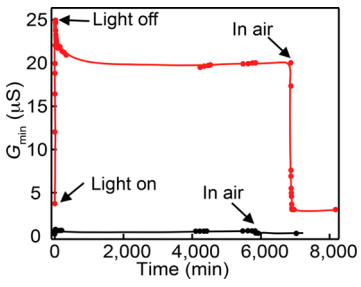

Figure 6. CNP conductance (G_{min}) as a function of time for $(rGO/Ti_{0.87}O_2^{0.52-})_{10}$ (red trace) and $(rGO)_{10}$ (black trace) during the whole UV illumination and dark process shown in Supporting Information Figure S3.

On the basis of the results, we may understand the enhanced conductance of the $(rGO/Ti_{0.87}O_2^{0.52-})_{10}$ film upon UV illumination and its persistency according to the schematic model illustrated in Figure 7. The channel in the FET has water and oxygen molecules adsorbed onto the surface when in air (I). In addition, the film intrinsically contains water molecules or oxonium ions in the intersheet gallery. These molecules persist, even upon evacuation, as has been discussed in previous studies.[36,48] When the device is illuminated with UV light, charge separation occurs in the $Ti_{0.87}O_2^{0.52-}$ nanosheets, and the generated electrons are transferred to rGO (II). A major portion of the positive holes in $Ti_{0.87}O_2^{0.52-}$ nanosheets having strong oxidative power are consumed in oxidizing water molecules, whereas some of electrons are involved in the reduction of oxygen molecules (III). When the illumination is terminated, the remaining holes are extinguished via recombination with electrons in rGO (IV). It is reasonable to assume that the number of adsorbed oxygen molecules is less than that of water molecules, considering the hydrophilic nature of $Ti_{0.87}O_2^{0.52-}$ nanosheets and the solution-based fabrication process of the superlattice film. Thus, there are more photogenerated electrons than holes, and a significant number of electrons survive (V), contributing to the enhanced conductance. The charge neutrality of the entire film may be maintained with protons, which are formed through the oxidative decomposition of water molecules with holes. The resulting system (V), or electrons accumulated in rGO, should be stable in vacuum, exhibiting the persistently enhanced conductance. The charge accumulation into niobate nanosheets has been reported.[49] However, this case is apparently different. The charge accumulation into niobate nanosheets proceeded in a colloidal system, while that in the present study was attained in rGO in the FET device.

CONCLUSIONS

In summary, the FET based on a superlattice hybrid film of rGO coupled with $Ti_{0.87}O_2^{0.52-}$ nanosheets exhibited distinctive modulation on electrical transport properties upon UV illumination. The device exhibited an n-type unipolar response, which changed from the ambipolar behavior observed prior to the irradiation. At the same time, the conductance was significantly enhanced by ∼7-fold. The enhancement, as well as the n-type unipolarity, is unique to the present device compared to the rather modest photomodulation reported for other graphene-based systems. These behaviors may be understood by the efficient transfer of photoexcited electrons in $Ti_{0.87}O_2^{0.52-}$ nanosheets to rGO. Interestingly, electrons in rGO could survive for a long time, showing the persistently enhanced conductance for days. This result may be regarded as effective charge storage, opening new applications for rGO or graphene.

The molecularly thin nature of $Ti_{0.87}O_2^{0.52-}$ nanosheets is well-suited to be hybridized with graphene, rGO, and other 2D

DOI: 10.1021/acsami.5b02107
ACS Appl. Mater. Interfaces 2015, 7, 11436−11443

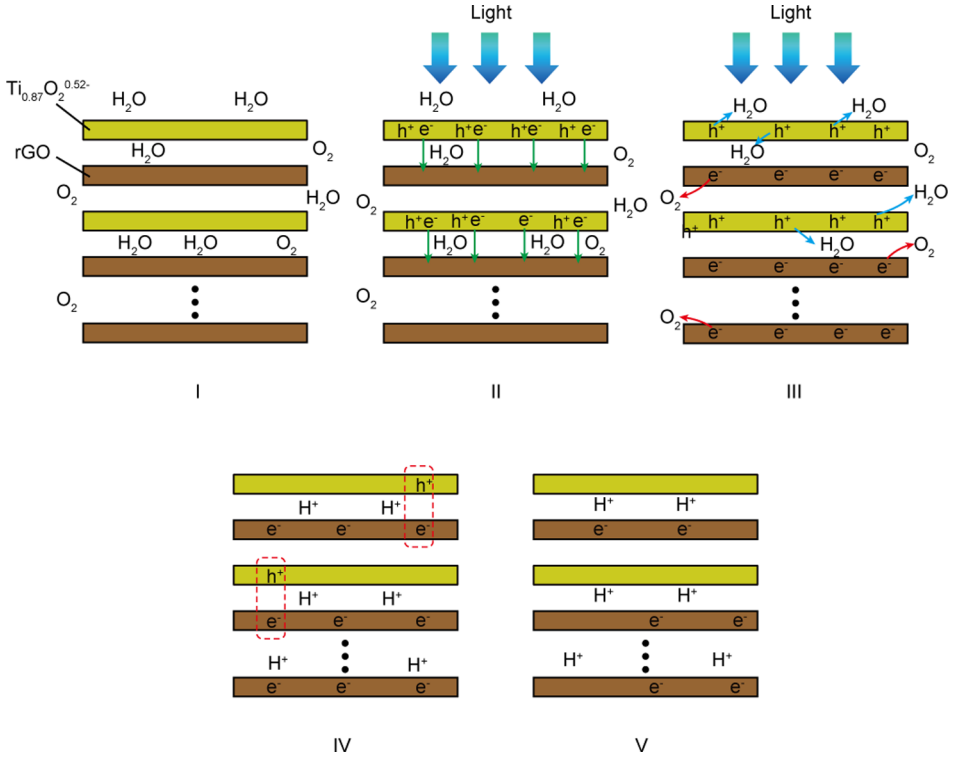

Figure 7. Schematic illustration of the enhanced conductance under UV illumination and its persistency. (I) Water and oxygen molecules are adsorbed in the channel of the FET devices. (II) Charge separation occurs in the $Ti_{0.87}O_2^{0.52-}$ nanosheets, and the generated electrons are transferred to rGO. (III) A large portion of the positive holes is consumed by oxidizing the adsorbed water molecules, whereas some portion of electrons is consumed by reducing oxygen molecules. (IV) Remaining holes are extinguished via recombination with electrons in rGO. (V) The excessive electrons survive, contributing to the enhanced conductance.

materials because the intimate contact at a molecular level can be achieved via facile solution processes. Such an aspect, as well as the highly photoresponsive nature, will be beneficial for the photomodulation of graphene transistor devices.

■ ASSOCIATED CONTENT

Supporting Information

AFM images of GO and $Ti_{0.87}O_2^{0.52-}$ nanosheets, UV−vis absorption spectra in the multilayer buildup process, conductance changes under different light illumination conditions, $G-V$ curves of $(rGO)_{10}$ after 20 min of UV illumination, series of $G-V$ curves under UV illumination and in the dark, and conductance change under prolonged UV illumination time. The Supporting Information is available free of charge on the ACS Publications website at DOI: 10.1021/acsami.5b02107.

■ AUTHOR INFORMATION

Corresponding Author

*E-mail: sasaki.takayoshi@nims.go.jp.

Author Contributions

The manuscript was written through contributions of all the authors. All the authors have given approval to the final version of the manuscript.

Notes

The authors declare no competing financial interest.

■ ACKNOWLEDGMENTS

This work was partly supported by the World Premier International Research Center Initiative on Materials Nanoarchitectonics (WPI-MANA), MEXT, Japan, and CREST of the Japan Science and Technology Agency (JST).

■ REFERENCES

(1) Novoselov, K. S.; Geim, A. K.; Morozov, S. V.; Jiang, D.; Zhang, Y.; Dubonos, S. V.; Grigorieva, I. V.; Firsov, A. A. Electric Field Effect in Atomically Thin Carbon Films. *Science* **2004**, *306*, 666−669.

(2) Geim, A. K. Graphene: Status and Prospects. *Science* **2009**, *324*, 1530−1534.

(3) Lee, C.; Wei, X.; Kysar, J. W.; Hone, J. Measurement of the Elastic Properties and Intrinsic Strength of Monolayer Graphene. *Science* **2008**, *321*, 385−388.

(4) Eda, G.; Fanchini, G.; Chhowalla, M. Large-Area Ultrathin Films of Reduced Graphene Oxide As a Transparent and Flexible Electronic Material. *Nat. Nanotechnol.* **2008**, *3*, 270−274.

(5) Geim, A. K.; Novoselov, K. S. The Rise of Graphene. *Nat. Mater.* **2007**, *6*, 183−191.

(6) Ahn, J.-H.; Hong, B. H.; Torrisi, F.; Coleman, J. N.; Liu, J.; Böhm, S.; Drndić, M.; Kostarelos, K.; Novoselov, K. S.; Siochi, E. J. Things You Could Do With Graphene. *Nat. Nanotechnol.* **2014**, *9*, 737−747.

(7) Ma, R.; Sasaki, T. Nanosheets of Oxides and Hydroxides: Ultimate 2D Charge-Bearing Functional Crystallites. *Adv. Mater.* **2010**, *22*, 5082−5104.

(8) Osada, M.; Sasaki, T. Two-Dimensional Dielectric Nanosheets: Novel Nanoelectronics from Nanocrystal Building Blocks. *Adv. Mater.* **2012**, *24*, 210−228.

(9) Wang, L. Z.; Sasaki, T. Titanium Oxide Nanosheets: Graphene Analogues with Versatile Functionalities. *Chem. Rev.* **2014**, *114*, 9455−9486.

(10) Xu, M.; Liang, T.; Shi, M.; Chen, H. Graphene-Like Two-Dimensional Materials. *Chem. Rev.* **2013**, *113*, 3766−3798.

DOI: 10.1021/acsami.5b02107
ACS Appl. Mater. Interfaces 2015, 7, 11436−11443

(11) Dean, C. R.; Young, A. F.; Meric, I.; Lee, C.; Wang, L.; Sorgenfrei, S.; Watanabe, K.; Taniguchi, T.; Kim, P.; Shepard, K. L.; Hone, J. Boron Nitride Substrates for High-Quality Graphene Electronics. *Nat. Nanotechnol.* **2010**, *5*, 722−726.
(12) Radisavljevic, B.; Radenovic, A.; Brivio, J.; Giacometti, V.; Kis, A. Single-Layer MoS_2 Transistors. *Nat. Nanotechnol.* **2011**, *6*, 147−150.
(13) Wang, Q. H.; Kalantar-Zadeh, K.; Kis, A.; Coleman, J. N.; Strano, M. S. Electronics and Optoelectronics of Two-Dimensional Transition Metal Dichalcogenides. *Nat. Nanotechnol.* **2012**, *7*, 699−712.
(14) Wu, W.; Wang, L.; Li, Y.; Zhang, F.; Lin, L.; Niu, S.; Chenet, D.; Zhang, X.; Hao, Y.; Heinz, T. F.; Hone, J.; Wang, Z. L. Piezoelectricity of Single-Atomic-Layer MoS_2 for Energy Conversion and Piezotronics. *Nature* **2014**, *514*, 470−474.
(15) Geim, A. K.; Grigorieva, I. V. Van der Waals Heterostructures. *Nature* **2013**, *499*, 419−425.
(16) Wang, L.; Meric, I.; Huang, P. Y.; Gao, Q.; Gao, Y.; Tran, H.; Taniguchi, T.; Watanabe, K.; Campos, L. M.; Muller, D. A.; Guo, J.; Kim, P.; Hone, J.; Shepard, K. L.; Dean, C. R. One-Dimensional Electrical Contact to a Two-Dimensional Material. *Science* **2013**, *342*, 614−617.
(17) Dean, C. R.; Wang, L.; Maher, P.; Forsythe, C.; Ghahari, F.; Gao, Y.; Katoch, J.; Ishigami, M.; Moon, P.; Koshino, M.; Taniguchi, T.; Watanabe, K.; Shepard, K. L.; Hone, J.; Kim, P. Hofstadter's Butterfly and the Fractal Quantum Hall Effect in Moiré Superlattices. *Nature* **2013**, *497*, 598−602.
(18) Yu, W. J.; Li, Z.; Zhou, H.; Chen, Y.; Wang, Y.; Huang, Y.; Duan, X. Vertically Stacked Multi-Heterostructures of Layered Materials for Logic Transistors and Complementary Inverters. *Nat. Mater.* **2013**, *12*, 246−252.
(19) Ju, L.; Velasco, J., Jr; Huang, E.; Kahn, S.; Nosiglia, C.; Tsai, H.-Z.; Yang, W.; Taniguchi, T.; Watanabe, K.; Zhang, Y.; Zhang, G.; Crommie, M.; Zettl, A.; Wang, F. Photoinduced Doping in Heterostructures of Graphene and Boron Nitride. *Nat. Nanotechnol.* **2014**, *9*, 348−352.
(20) Ma, R.; Sasaki, T. Two-Dimensional Oxide and Hydroxide Nanosheets: Controllable High-Quality Exfoliation, Molecular Assembly, and Exploration of Functionality. *Acc. Chem. Res.* **2015**, *48*, 136−143.
(21) Sasaki, T. Fabrication of Nanostructured Functional Materials Using Exfoliated Nanosheets as a Building Block. *J. Ceram. Soc. Jpn.* **2007**, *115*, 9−16.
(22) Sasaki, T.; Ebina, Y.; Tanaka, T.; Harada, M.; Watanabe, M.; Decher, G. Layer-by-Layer Assembly of Titania Nanosheet/Polycation Composite Films. *Chem. Mater.* **2001**, *13*, 4661−4667.
(23) Akatsuka, K.; Haga, M.; Ebina, Y.; Osada, M.; Fukuda, K.; Sasaki, T. Construction of Highly Ordered Lamellar Nanostructures through Langmuir−Blodgett Deposition of Molecularly Thin Titania Nanosheets Tens of Micrometers Wide and Their Excellent Dielectric Properties. *ACS Nano* **2009**, *3*, 1097−1106.
(24) Cai, X.; Ma, R.; Ozawa, T. C.; Sakai, N.; Funatsu, A.; Sasaki, T. Superlattice Assembly of Graphene Oxide (GO) and Titania Nanosheets: Fabrication, In Situ Photocatalytic Reduction of GO and Highly Improved Carrier Transport. *Nanoscale* **2014**, *6*, 14419−14427.
(25) Hummers, W. S.; Offeman, R. E. Preparation of Graphitic Oxide. *J. Am. Chem. Soc.* **1958**, *80*, 1339.
(26) Sasaki, T.; Watanabe, M.; Hashizume, H.; Yamada, H.; Nakazawa, H. Macromolecule-like Aspect for a Colloidal Suspension of an Exfoliated Titanate. Pairwise Association of Nanosheets and Dynamic Reassembling Process Initiated from It. *J. Am. Chem. Soc.* **1996**, *118*, 8329−8335.
(27) Sasaki, T.; Ebina, Y.; Fukuda, K.; Tanaka, T.; Harada, M.; Watanabe, M. Titania Nanostructured Films Derived from a Titania Nanosheet/Polycation Multilayer Assembly via Heat Treatment and UV Irradiation. *Chem. Mater.* **2002**, *14*, 3524−3530.
(28) Osada, M.; Ebina, Y.; Funakubo, H.; Yokoyama, S.; Kiguchi, T.; Takada, K.; Sasaki, T. High-*k* Dielectric Nanofilms Fabricated from Titania Nanosheets. *Adv. Mater.* **2006**, *18*, 1023−1027.
(29) Kim, Y. D.; Bae, M.-H.; Seo, J.-T.; Kim, Y. S.; Kim, H.; Lee, J. H.; Ahn, J. R.; Lee, S. W.; Chun, S.-H.; Park, Y. D. Focused-Laser-Enabled p−n Junctions in Graphene Field-Effect Transistors. *ACS Nano* **2013**, *7*, 5850−5857.
(30) Tang, Y.-B.; Lee, C.-S.; Xu, J.; Liu, Z.-T.; Chen, Z.-H.; He, Z.; Cao, Y.-L.; Yuan, G.; Song, H.; Chen, L.; Luo, L.; Cheng, H.-M.; Zhang, W.-J.; Bello, I.; Lee, S.-T. Incorporation of Graphenes in Nanostructured TiO_2 Films via Molecular Grafting for Dye-Sensitized Solar Cell Application. *ACS Nano* **2010**, *4*, 3482−3488.
(31) Sakai, N.; Ebina, Y.; Takada, K.; Sasaki, T. Electronic Band Structure of Titania Semiconductor Nanosheets Revealed by Electrochemical and Photoelectrochemical Studies. *J. Am. Chem. Soc.* **2004**, *126*, 5851−5858.
(32) Xiang, Q.; Yu, J. Graphene-Based Photocatalysts for Hydrogen Generation. *J. Phys. Chem. Lett.* **2013**, *4*, 753−759.
(33) Xiang, Q.; Yu, J.; Jaroniec, M. Enhanced Photocatalytic H_2-Production Activity of Graphene-Modified Titania Nanosheets. *Nanoscale* **2011**, *3*, 3670−3678.
(34) Xiang, Q.; Yu, J.; Jaroniec, M. Graphene-Based Semiconductor Photocatalysts. *Chem. Soc. Rev.* **2012**, *41*, 782−796.
(35) Williams, G.; Seger, B.; Kamat, P. V. TiO_2-Graphene Nanocomposites. UV-Assisted Photocatalytic Reduction of Graphene Oxide. *ACS Nano* **2008**, *2*, 1487−1491.
(36) Eda, G.; Chhowalla, M. Chemically Derived Graphene Oxide: Towards Large-Area Thin-Film Electronics and Optoelectronics. *Adv. Mater.* **2010**, *22*, 2392−2415.
(37) Ryu, S.; Liu, L.; Berciaud, S.; Yu, Y.-J.; Liu, H.; Kim, P.; Flynn, G. W.; Brus, L. E. Atmospheric Oxygen Binding and Hole Doping in Deformed Graphene on a SiO_2 Substrate. *Nano Lett.* **2010**, *10*, 4944−4951.
(38) Late, D. J.; Liu, B.; Matte, H. S. S. R.; Dravid, V. P.; Rao, C. N. R. Hysteresis in Single-Layer MoS_2 Field Effect Transistors. *ACS Nano* **2012**, *6*, 5635−5641.
(39) Han, J. T.; Kim, B. J.; Kim, B. G.; Kim, J. S.; Jeong, B. H.; Jeong, S. Y.; Jeong, H. J.; Cho, J. H.; Lee, G.-W. Enhanced Electrical Properties of Reduced Graphene Oxide Multilayer Films by In-Situ Insertion of a TiO_2 Layer. *ACS Nano* **2011**, *5*, 8884−8891.
(40) Maeng, J.; Park, W.; Choe, M.; Jo, G.; Kahng, Y. H.; Lee, T. Transient Drain Current Characteristics of ZnO Nanowire Field Effect Transistors. *Appl. Phys. Lett.* **2009**, *95*, 123101.
(41) The G_{min} can be further improved by the prolonged UV illumination time (Supporting Information Figure S6). The final enhancement was 6−10-fold for different devices.
(42) Eda, G.; Chhowalla, M. Graphene-Based Composite Thin Films for Electronics. *Nano Lett.* **2009**, *9*, 814−818.
(43) Kobayashi, T.; Kimura, N.; Chi, J.; Hirata, S.; Hobara, D. Channel-Length-Dependent Field-Effect Mobility and Carrier Concentration of Reduced Graphene Oxide Thin-Film Transistors. *Small* **2010**, *6*, 1210−1215.
(44) Wang, S.; Chia, P.-J.; Chua, L.-L.; Zhao, L.-H.; Png, R.-Q.; Sivaramakrishnan, S.; Zhou, M.; Goh, R.G.-S.; Friend, R. H.; Wee, A. T.-S.; Ho, P. K.-H. Band-Like Transport in Surface Functionalized Highly Solution-Processable Graphene Nanosheets. *Adv. Mater.* **2008**, *20*, 3440−3446.
(45) Yun, J. M.; Park, S.; Hwang, Y. H.; Lee, E.-S.; Maiti, U.; Moon, H.; Kim, B.-H.; Bae, B.-S.; Kim, Y.-H.; Kim, S. O. Complementary p- and n-Type Polymer Doping for Ambient Stable Graphene Inverter. *ACS Nano* **2014**, *8*, 650−656.
(46) Upon exposure to the air, the conductance returned back to the value before UV illumination (Figure 6), suggesting that the accumulated photoelectrons in rGO are consumed by oxidative agents in air. If we evacuate the chamber and illuminate the device again, the conductance enhancement was reproduced.
(47) Zhao, X.; Liu, Z.-B.; Yan, W.-B.; Wu, Y.; Zhang, X.-L.; Chen, Y.; Tian, J.-G. Ultrafast Carrier Dynamics and Saturable Absorption of Solution-Processable Few-Layered Graphene Oxide. *Appl. Phys. Lett.* **2011**, *98*, 121905.

DOI: 10.1021/acsami.5b02107
ACS Appl. Mater. Interfaces 2015, 7, 11436−11443

(48) Jung, I.; Dikin, D. A.; Piner, R. D.; Ruoff, R. S. Tunable Electrical Conductivity of Individual Graphene Oxide Sheets Reduced at "Low" Temperatures. *Nano Lett.* **2008**, *8*, 4283−4287.
(49) Nakato, T.; Yamada, Y.; Miyamoto, N. Photoinduced Charge Separation in a Colloidal System of Exfoliated Layered Semiconductor Controlled by Coexisting Aluminosilicate Clay. *J. Phys.Chem. B* **2009**, *113*, 1323−1331.

DOI: 10.1021/acsami.5b02107
ACS Appl. Mater. Interfaces 2015, 7, 11436−11443